Reduced Dimensionality Quantum Dynamics of $CH_3 + CH_4 \rightarrow CH_4 + CH_3$: Symmetric Hydrogen Exchange on an Ab Initio Potential†

Sarah M. Remmert,* Simon T. Banks,* and David C. Clary*

Department of Chemistry, University of Oxford, PTCL, South Parks Road, Oxford, OX13QZ, United Kingdom

Received: December 8, 2008; Revised Manuscript Received: January 18, 2009

The symmetric title reaction $CH_3 + CH_4 \rightarrow CH_4 + CH_3$ is studied using quantum scattering theory. Quantum dynamics calculations are performed in hyperspherical coordinates with a two-dimensional effective potential energy surface consisting of an analytical 18-parameter double Morse function fit to ab initio data at the CCSD(T)/cc-pVTZ//MP2/cc-pVTZ level of theory. Spectator modes are treated adiabatically by inclusion of projected zero-point energy corrections in the effective potential. The close-coupled equations are solved via *R*-matrix propagation. Energy and J-shifted thermal rate constants are compared to experimental data and highlight the importance of quantum tunneling. Oscillating reactivity and metastable bound state resonances are observed in the cumulative and state-to-state reaction probabilities. State-to-state differential and initial state-selected integral cross sections are presented and discussed. Primary and secondary kinetic isotope effects for two symmetric deuterated variants of the title reaction are also presented.

Introduction

Reactions of the type $CH_3 + RH \rightarrow CH_4 + R$ are thought to be essential for hydrocarbon combustion and thermal decomposition processes.[1] Despite their importance, many of these elementary hydrocarbon reactions are not well understood. As accurate characterization of the rate constants for elementary hydrocarbon reactions is important in modeling the mechanism of combustion processes, continued detailed quantum analyses of these reactions are therefore important for the development of reaction models.

The symmetric hydrogen exchange:

$$CH_3 + CH_4 \rightarrow CH_4 + CH_3 \qquad (1)$$

is the simplest reaction of type $CH_3 + RH$, and has been used, in combination with the methyl + ethane reaction, as a model from which to interpret the properties of the entire reaction class.[2] This heavy−light−heavy (HLH) reaction has been the focus of many previous experimental and theoretical characterizations. Several experimental studies have been done on this system and isotopic variants,[3−7] although, because of symmetry considerations, all of these experiments were indirect measurements involving derivation of a suitable rate constant by comparison with the rate of a well-characterized reference reaction. Kerr and Parsonage,[8] and Arthur and Bell[9] both independently presented useful evaluations of kinetic experiments prior to 1974 and 1977, respectively. Kerr suggests a "best" estimate of the thermal rate constant on the order of 10^{-19} to 10^{-17}cm^3 molecule^{-1} s^{-1} (450−800 K), with up to 30% estimated error limits.

Numerous electronic structure and transition state theory (TST) studies have also been done, both in isolation and as a foundation from which to consider larger hydrocarbon hydrogen abstraction processes.[2,10−17] The most sophisticated treatment of the reaction rate of the system was recently presented by Kungwan et al., who reported the importance of tunneling to the reaction rate by a canonical variational transition state theory (CVT) study with a small curvature tunneling (SCT) correction.[2] The large quantum tunneling contribution, in combination with uncertainty in the experimental data, suggests the need for a higher order quantum treatment of the system to accurately predict reaction rates. This is especially true in the low temperature regime where, to the best of our knowledge, no experimental data exists. This study focuses on characterizing the reaction kinetics and reduced dimensionality (RD) quantum dynamics of the title reaction (1) and two deuterated variations, probed to investigate primary (2) and secondary (3) kinetic isotope effects (KIEs):[10]

$$CH_3 + CH_3D \rightarrow CH_3D + CH_3 \qquad (2)$$

$$CD_3 + CD_4 \rightarrow CD_4 + CD_3 \qquad (3)$$

In addition to the importance of characterizing the rate of the title reaction, the system also presents the opportunity to extend the application of an RD method hitherto restricted primarily to atom−molecule collisions.[18−21] While full dimensional quantum scattering calculations produce exact detailed kinetic and dynamical information, inclusion of the full $3N - 6$ internal degrees of freedom—in combination with treatment of molecular rotation—is not feasible in a method requiring the explicit computation of state-to-state transition probabilities.[22] This computational bottleneck is augmented by the problem of accurately describing the multidimensional reaction potential for the system; expensive full $3N - 6$ dimensional potential energy surfaces (PES) are mainly restricted to systems of four atoms or less,[22,23] although full potentials have, for example, been developed for reactions involving up to nine atoms.[24]

TST and modifications thereof have been extensively used to model reaction kinetics where the number of degrees of freedom exceeds the capacity of full dimensional scattering

† Part of the "George C. Schatz Festschrift".

* Corresponding author. E-mail: sarah.remmert@chem.ox.ac.uk; simon.banks@chem.ox.ac.uk; david.clary@chem.ox.ac.uk.

10.1021/jp810803k CCC: $40.75
Published on Web 03/02/2009

techniques. TST-based methods, although inherently classical in nature, may be viewed as a hierarchy upon which successive inclusion of sophisticated quantum tunneling corrections bridges the gap to accurate quantum scattering theory results.[25] Quantum RD methods combine the accuracy of exact calculations for a subset of active degrees of freedom with the efficiency of TST approximations for the remaining, spectator modes.[26,27] RD methods are therefore an improvement upon TST approaches in describing the influence of quantum effects, such as hydrogen tunneling and high-temperature recrossing, on the reaction kinetics.

The two-dimensional (2D) method implemented here has been applied successfully in a number of recent studies,[18−20,28] including the HLH reaction Cl + HCH_3.[21] The method is essentially an extension to higher dimensions of the Bending Corrected Rotating Linear Model (BCRLM) of Walker and Hayes,[29] defined by a collinear reaction path, linear rigid rotor treatment of total molecular rotation, and adiabatic energy corrections for the $3N - 8$ spectator modes not treated explicitly in the quantum scattering calculations. A recent improvement of this method was the incorporation of an ab initio-driven development of a 2D PES.[18] Subsequent method development in rigorously determining the adiabatic zero-point energy corrections (ZPEs) for the spectator modes has dramatically improved this ab initio RD approach.[30]

This paper is presented as follows: the 2D Hamiltonian and hyperspherical coordinate systems are defined, development of the potential surface is discussed, and solution of the close-coupled equations is presented. Results and conclusions are subsequently given.

Background Theory

Hyperspherical Coordinates. The 2D method implemented here relies on division of the system internal degrees of freedom into two distinct subsets: the two active modes associated with bond formation and breaking that are treated explicitly in the quantum scattering calculations, and the remaining $3N - 8$ spectator modes that are treated via an adiabatic correction with an effective PES.[18] For the purposes of this work, we will refer to all internal motions as vibrations.

Active-mode vibrations are described in hyperspherical coordinates, according to motion in the hyperspherical angle δ and the hyperspherical radius ρ. The use of these coordinates in the present case is justified by the HLH nature of the reaction: adiabatic separation between the "slow" variable ρ (approximately pertaining to the heavy atom separation) and the "fast" variable δ (approximately the separation between the transferring hydrogen and the abstracting species) increases as the skewing angle, δ_{max}, decreases.[31] Hyperspherical coordinates have the additional advantage of allowing a smooth description of the reaction system as it traverses along the reaction path, although coordinate transformation is necessary for the accurate application of boundary conditions. Hyperspherical coordinates are defined according to the usual convention from the product Jacobi coordinates shown in Figure 1.

R_1 is defined as the center of mass distance between the two product species, $CH_3(1)$ and $H_aCH_3(2)$, while R_2 is given as the distance between the center of mass of $CH_3(2)$ and H_a. The hyperspherical radius, ρ, and angle, δ, are calculated according to

$$\frac{M_1}{\mu}R_1^{\,2} = [\rho\cos(\delta)]^2 \tag{4}$$

$$\frac{M_2}{\mu}R_2^{\,2} = [\rho\sin(\delta)]^2 \tag{5}$$

where the reduced masses are defined as[18,32]

$$M_1 = \frac{(m_{CH_3(1)})(m_{CH_3(2)} + m_{H_a})}{m_{tot}} \tag{6}$$

$$M_2 = \frac{(m_{H_a})(m_{CH_3(2)})}{m_{H_a} + m_{CH_3(2)}} \tag{7}$$

$$M_3 = \frac{(m_{C(1)})(m_{H_3(1)})}{m_{CH_3(1)}} \tag{8}$$

$$\mu = (M_1M_2M_3)^{1/3} \tag{9}$$

with skewing angle, δ_{max}:

$$\delta_{max} = \arctan\left(\sqrt{\frac{m_{H_a}m_{tot}}{m_{CH_3(1)}m_{CH_3(2)}}}\right) \tag{10}$$

Hamiltonian and Method Outline. The RD Hamiltonian operator for the active modes (scaled by $\rho^{-3/2}$ for ease of solution[29]) is given as (in atomic units)

$$\hat{H} = -\frac{1}{2\mu}\frac{\partial^2}{\partial\rho^2} - \frac{1}{2\mu\rho^2}\frac{\partial^2}{\partial\delta^2} + \frac{3}{8\mu\rho^2} + \frac{\hat{J}^2}{2\mu\rho^2} + V(\rho,\delta) \tag{11}$$

Solution of the time-independent RD Schrödinger equation is achieved as follows. A grid in hyperspherical coordinates of high-level ab initio calculations is developed, and spectator-mode ZPEs are determined after projecting contributions from the active modes out of the Hessian. These ZPEs are then added to ab initio energies, and an analytical function is fitted to the resulting grid. The close-coupled equations are solved via the R-matrix propagation method of Stechel, Walker, and Light,[33] and the application of approximate boundary conditions affords a simple approach to the evaluation of the reaction probability. These steps are outlined in the following sections.

System Energetics

Stationary Points. All stationary point geometry optimizations and frequency calculations were performed at the MP2/cc-pVTZ level of theory with CCSD(T)/cc-pVTZ single-point energy calculations. Calculations were run with the Gaussian

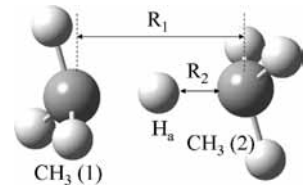

Figure 1. Product Jacobi coordinates for the CH_3 + CH_4 reaction. H_a transfers from $CH_3(1)$ to $CH_3(2)$ along a collinear abstraction pathway.

TABLE 1: Harmonic Frequencies for Stationary Points at the MP2/cc-pVTZ Level (in cm^{-1})[a]

species	frequencies					
CH_3	486.2	1445.4	1445.5	3177.9	3368.9 (2)	
CH_4	1350.1 (3)	1586.3 (2)	3075.0	3210.8 (3)		
CD_3	376.9	1063.5 (2)	2248.0	2510.8 (2)		
CD_4	1020.5 (3)	1122.1 (2)	2175.2	2377.3 (3)		
CH_3D	1193.3 (2)	1344.3	1522.1 (2)	2321.3	3115.0	3210.5 (2)
TS1 (pre)	1949.8 *i*	48.5	322.5 (2)	540.8	706.2 (2)	1164.5
	1197.7	1375.7 (2)	1463.1 (2)	1489.9 (2)	3109.2	3110.6
	3257.4 (2)	3257.8 (2)				
TS1 (post)	48.5	322.5 (2)	706.2(2)	1052.3	1074.6	1375.7(2)
	1463.1(2)	1489.9(2)	3090.0	3109.2	3257.4(2)	3257.8(2)
TS2 (pre)	1454.0 *i*	48.5	295.8 (2)	540.8	706.2 (2)	1098.1 (2)
	1154.5	1164.5	1462.9 (2)	1463.1 (2)	3108.8	3110.6
	3257.4 (2)	3257.8 (2)				
TS2 (post)	48.5	295.8 (2)	706.2 (2)	1052.3	1070.8	1098.1 (2)
	1462.9 (2)	1463.1 (2)	3090.0	3108.5	3257.4 (2)	3257.8 (2)
TS3 (pre)	1434.5 *i*	34.3	228.6 (2)	477.0	528.7 (2)	897.0
	927.1	1012.8 (2)	1065.5 (2)	1066.5 (2)	2212.4	2216.7
	2419.4 (2)	2420.0 (2)				
TS3 (post)	34.3	228.6 (2)	528.7 (2)	744.4	820.7	1012.8 (2)
	1065.5 (2)	1066.5 (2)	2185.8	2212.2	2419.4 (2)	2420.0 (2)

[a] Multiplicities in parentheses. TS frequencies are given prior to (pre) and following (post) projection out of explicitly treated vibrational modes. TS1, TS2, and TS3 refer to the TSs of reactions 1, 2, and 3, respectively.

03 electronic structure package,[34] and symmetry constraints were not imposed at any point. Stationary point geometries (Figure 2) and frequencies (Table 1) are in good agreement with previous theoretical studies, including QCISD/cc-pVDZ characterization of the transition state (TS).[2] Reactant molecules are optimized separately by assuming infinite separation in the asymptotic region. Reaction energetics are shown in Table 2, where ΔV is given as the energy difference between the TS and the reactants, and ΔV_a^G is the corresponding zero-point corrected energy difference. An intrinsic reaction coordinate (IRC) calculation confirmed the absence of any other stationary points along the minimum energy path (MEP) and the presence of a collinear reaction pathway. Rotational symmetry numbers (σ) and moments of inertia (I) are given in Table 3.

Potential Energy Surface Development. MP2/cc-pVTZ//CCSD(T)/cc-pVTZ ab initio grid points were obtained by constraining molecular geometry at fixed values of R_1 and R_2 while allowing all spectator modes to relax. Grid points were generated for δ values in the interval $\delta = 0 \rightarrow \delta_{max}$ at fixed slices of ρ ranging from the $\rho = 8.87$ TS to an asymptotically large value of $\rho = 15$. Grid points along the MEP (determined via an IRC calculation), as well as approximately perpendicular to the MEP at the TS saddle point (from $\rho = 7.4$ to $\rho = 15$), were obtained. The symmetry of the title reaction was used such that only 1/2 of the necessary grid calculations for a nonsymmetric system were required.

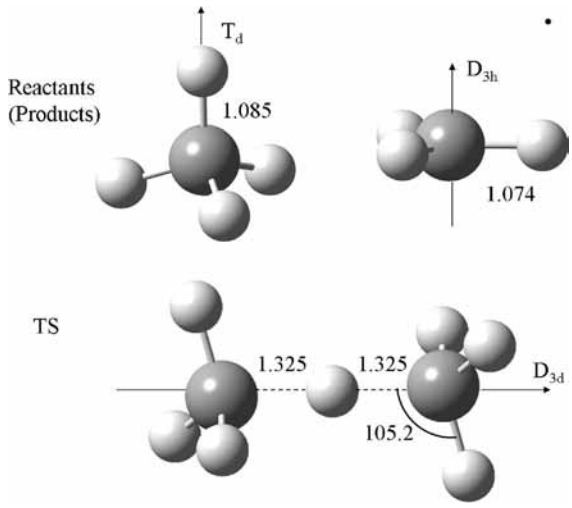

Figure 2. Reaction stationary points for the $CH_3 + CH_4$ reaction. Bond lengths and angles given in a.u. and degrees, respectively.

TABLE 2: Single-Point Energies and ZPEs for Reaction Stationary Points at the CCSD(T)/cc-pVTZ//MP2/cc-pVTZ Level

	energies	ZPE
Molecular Energies (in hartree)		
CH_3	−39.760937548	0.030283
CH_4	−40.438068280	0.045404
$CH_3-H_a-CH_3$ (TS)	−80.170094430	0.074990
CD_3	−39.760937548	0.0222811
CD_4	−40.438068280	0.0333135
CH_3D	−40.438068280	0.0424771
CH_3-D-CH_3 (TS1)	−80.170094430	0.0734312
CD_3-D-CD_3 (TS2)	−80.170094430	0.0552778
Reaction Energetics (in kcal/mol, quantities defined in text)		
ΔV (TS1)	18.1421769	
ΔV_a^G (TS1)	17.70480278	
ΔV_a^G (TS2)	18.56329853	
ΔV_a^G (TS3)	17.93218085	

TABLE 3: Rotational Moments of Inertia (amu × $bohr^2$)

species	point group	σ	I_a	I_b	I_c
CH_3	D_{3h}	6	6.23157	6.23224	12.46381
CH_4	T_d	12	11.30851	11.30851	11.30851
TS1	D_{3d}	6	23.59303	218.16295	218.16295
CH_3D	C_{3v}	3	11.30851	15.29260	15.29260
CD_4	T_d	12	22.59964	22.59964	22.59964
CD_3	D_{3h}	6	12.45357	12.45491	24.90848
TS2	D_{3d}	6	23.59302	218.16294	218.16294
TS3	D_{3d}	6	47.14981	285.72845	285.72846

TABLE 4: Potential Energy Function Definitions (For Symmetric Systems, $f(\rho) = f'(\rho)$, $g(\rho) = g'(\rho)$, and $c = c'$)

	expression	description
$f(\rho)$	$(1 + c_1(\rho)^{c_2}e^{c_3(\rho)})c_4$	TS location
$f'(\rho)$	$(1 + c_{18}(\rho)^{c_{19}}e^{c_{20}(\rho)})c_{21}$	
$g(\rho)$	$c_5 + c_6\rho + c_7\rho^2$	well width
$g'(\rho)$	$c_{22} + c_{23}\rho + c_{24}\rho^2$	
$h(\rho)$	$((c_8 + c_9\rho + c_{10}\rho^2) - \log(c_{11} + c_{12}\rho + c_{13}\rho^2))/(c_{14} + c_{15}\rho + c_{16}\rho^2)$	δ_{min} location
$h'_{(symm)}$	$\delta_{max} - h(\rho)$	
$h'_{(asymm)}$	$((c_{25} + c_{26}\rho + c_{27}\rho^2) - \log(c_{28} + c_{29}\rho + c_{30}\rho^2))/(c_{31} + c_{32}\rho + c_{33}\rho^2)$	
c	c_{17}	well depth
c'	c_{34}	
c''_{symm}	c_{18}	Z-translation
c''_{asymm}	c_{35}	

The T1 diagnostic[35−37] was evaluated for each single point CCSD(T) calculation to judge the applicability of a single reference approach. The diagnostic was seen to range from values of 0.01 in the interaction region to 0.06 for large ρ, indicating that the accuracy of the system energy decreases in the asymptotic region. However, the T1 diagnostic values in the interaction region and along the MEP remained below the recommended 0.02 value[37] and thus justified the use of the CCSD(T) single reference energy method.

Adiabatic correction via an effective potential requires that each grid point energy value includes a ZPE for the spectator (but not active) modes. The contribution of the active modes was projected from the Hessian for nonstationary points in curvilinear internal coordinates according to a recently developed method;[30] to apply this method, four additional partial geometry optimizations were performed for each grid point for $\pm$ 0.001Å R_1 and R_2 perturbations.[30] This implementation assumes that projection of the hyperspherical coordinate spectator modes can be adequately approximated by projection relative to fixed Jacobi coordinates. The improvement of using this projection scheme in comparison to a rectilinear projection method[38] is considerable, and comparison of the two approaches for this system will be the focus of future work.

The effect of projection of active mode contributions in the rectilinear approach can be shown in Table 1, where the original and projected harmonic frequency TS values are shown. [As the TS is a stationary point, the curvilinear and rectilinear projection schemes should yield identical results. However, as the choice of coordinates used in application of the curvilinear projection neglects internal rotation, the smallest mode of 48.5 cm^{-1} is absent. For the surface grid points, the approximation is made that this mode has minimal contribution; however, in evaluation of the partition functions for determination of reaction rate, the full $3N - 6$ modes of the rectilinear projection scheme are used.] In general, there is little coupling between active and spectator modes, thereby validating the application of the 2D method described here. However, projection of $-1949.8i$ and 540.7 cm^{-1} modes does reduce modes at 1164.5 and 1197.7 cm^{-1} by 9.6% and 10.3%, respectively. These modes correspond to the umbrella motion of the CH_3 groups (with vibration of H_a for the 1197.7 cm^{-1} mode), and therefore some degree of coupling with the active modes is expected. There is also minor coupling associated with the symmetric CH_3 stretch at 3110.6 cm^{-1} due to motion of the carbon atoms along the D_{3d} axis, which leads to a 0.6% reduction in frequency wavenumber upon projection. The reduction of these three modes due to coupling likely causes a decrease in the ZPEs across the potential, $V(\rho, \delta)$ (i.e., 5.8×10^{-4} a.u. at TS).

ZPE-corrected grid points were fitted to an analytical function adapted from a previously used form.[18] Modification of this potential function can be performed with the retention of four key properties: (i) the presence of a saddle point at the TS, (ii) double Morse behavior as $\rho \rightarrow \infty$, (iii) $V(\rho, \delta) \rightarrow \infty$ as $\delta \rightarrow 0$ (δ_{max}), and (iv) $V(\rho, \delta) \rightarrow \infty$ for $\rho < \rho_{TS}$, such that asymptotic values are approached with the correct form based on physical behavior. The general form of the modified 35-parameter potential function is given in eq 12, expressed in terms of functions in ρ defined in Table 4. For the symmetric title reaction and both deuterated systems, symmetry about $\delta_{max}/2$ was used to simplify the form of the potential (Table 4), such that only 18 parameters were required.

$$V(\rho, \delta) = f(\rho)[(1 - e^{g(\rho)(h(\rho)-\delta)})^2 - c] + f'(\rho)[(1 - e^{g'(\rho)(\delta-h'(\rho))})^2 - c'] + c'' \quad (12)$$

Low-energy scattering calculations require an extremely accurate potential fit for energies below the sum of the incident translational energy and the initial internal energy of the reactant species (E_0). Each potential surface was therefore fitted via a least-squares

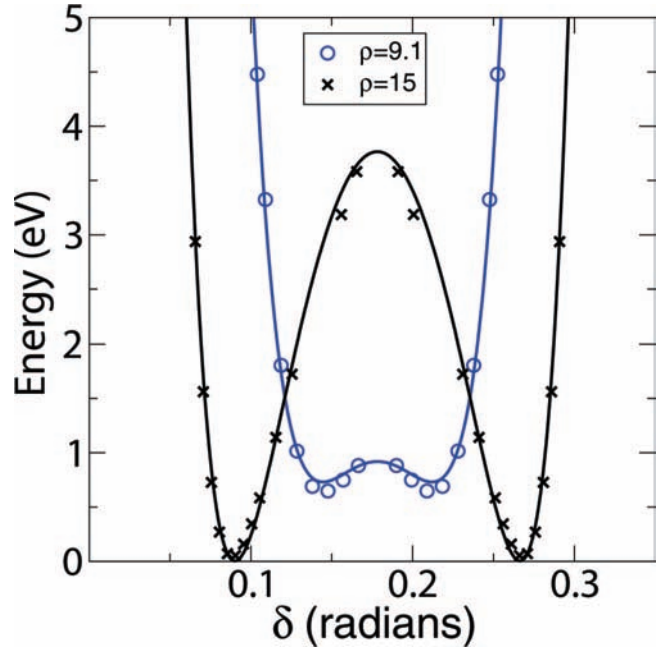

Figure 3. Fitted $V(\rho, \delta)$ (lines) and ab initio grid data (points) for values of ρ approximately pertaining to the asymptotic and interaction regions.

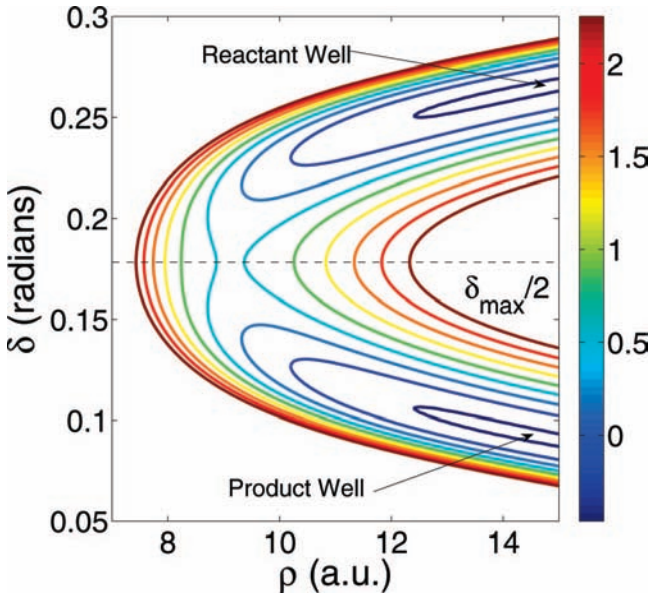

Figure 4. Contour diagram of the symmetric fitted potential $V(\rho, \delta)$ for the $CH_3 + CH_4$ reaction at hyperspherical coordinate values surrounding the TS. Relative energies for contour height, $E - E_0$, are given in eV.

procedure[39] following modification of individual parameters by eye and on the basis of physical significance (Table 4) to best reproduce the ab initio data. Convergence of the fitting procedure was monitored by evaluating the sum of the squared residuals (RSS), with adequate potential fits corresponding to RSS values on the order of 10^{-4} to 10^{-3}. For the deuterated reactions, determination of an adequate surface required a serial fitting procedure,[21] in which input parameters for a least-squares algorithm[39] were cycled through data sets capping the energy at subsequently lower values, above the level of the maximum energy accessible as a result of incident kinetic energy. For the title reaction, the potential yields an RSS value of 9.17×10^{-4}, and a total of 69 CCSD(T) calculations (138 grid points) were used in the fit. A visual representation of the quality of the fit is given in Figure 3. The symmetry of the potential function is shown in a contour diagram of the function in the interaction region (Figure 4). RSS values for deuterated reactions 2 and 3 were determined to be 1.18×10^{-3} and 1.49×10^{-3}, with 114 and 116 ab initio grid points used, respectively.

The parameters used for the title reaction surface are shown in Table 5 in addition to the surface parameters for deuterated reactions 2 and 3.

Scattering Theory

Solution of the Close-Coupled Equations. Once $V(\rho, \delta)$ has been established, the scattering Hamiltonian is solved by the inelastic scattering *R*-matrix propagation technique of Stechel, Walker, and Light.[33] The hyperspherical coordinate space is divided into even width sectors in ρ, and, at the center of each ρ sector (ρ_i), adiabatic separability between ρ and δ is assumed. Therefore, the δ-dependent Hamiltonian:

$$H_\delta = -\frac{1}{2\mu\rho_i^2}\frac{\partial^2}{\partial\delta^2} + V(\delta;\rho_i) \qquad (13)$$

is diagonalized using a discrete variable representation (DVR) with a particle-in-a-box basis[40] to yield hyperspherical adiabats (ε_i) and the δ-dependent wave functions ($\phi_k(\delta; \rho_i)$). In the event

TABLE 5: Potential Energy Surface Parameters

	$CH_3 + CH_4$	$CH_3 + CH_3D$	$CD_3 + CD_4$
c_1	12.170028	11.887985	11.102742
c_2	−0.350508	1.535278	−0.162939
c_3	−0.495922	−1.063911	−0.585622
c_4	1.013546	−2.488907	1.471863
c_5	2.524028	3.373061	2.209390
c_6	−0.086213	−0.131556	−0.084292
c_7	11.163709	11.459432	10.756782
c_8	0.415130	1.105082	1.059908
c_9	−0.008680	0.006073	−0.005795
c_{10}	8504.448780	8506.427598	8507.623653
c_{11}	1881.918008	1880.241117	1880.510465
c_{12}	−37.929645	−39.101582	−39.342152
c_{13}	0.016551	3.312355	5.214782
c_{14}	3.122611	1.529358	2.130098
c_{15}	0.052551	0.653112	0.482452
c_{16}	3.034464	3.526320	2.824825
c_{17}	−82.413065	−81.378561	−82.274405
c_{18}	0.324467	0.155136	0.321127

TABLE 6: Numerical Parameters

parameter	final value	description
ρ_{min}	7.4 au	first ρ sector (behind TS)
ρ_{max}	15 au	final asymptotic ρ sector
N_ρ	400	number of ρ sectors
S_{num}	60	number of ρ sectors to average $P_{ss'}$
N_δ	300	size of DVR basis
E_{max}	2.17 eV	maximum incident KE
E_{inc}	0.001 eV	energy grid spacing
N	16	contracted basis size
J_{max}	250	maximum angular momentum

of exact degeneracy, symmetrization of the DVR basis eigenfunctions is required in order to explicitly treat *gerade* and *ungerade* combinations of states.[41] In this study, degeneracy was instead lifted by adding a slight perturbation to $V(\rho, \delta)$ for $\delta > \delta_{max}/2$ (1×10^{-5} a.u.).

The expectation value of δ, $\langle\phi_k(\delta; \rho_i)|\delta|\phi_k(\delta; \rho_i)\rangle$ is used to classify the wave function state, k, as corresponding to reactant ($\langle\delta\rangle > \delta_{max}/2$) or product ($\langle\delta\rangle < \delta_{max}/2$) states in subsequent analysis.

The sector-dependent wave function for quantum state k is expanded as a function of ρ within a contracted basis of $\phi_{k'}(\delta; \rho_i)$ functions:

$$\Psi_k(\rho, \delta;\rho_i) = \sum_{k'}^{N} f_{k'k}(\rho;\rho_i)\phi_{k'}(\delta;\rho_i) \qquad (14)$$

where N is the size of the contracted basis, set to be larger than the number of open channels in the asymptotic region.[33]

Expressing the wave function in this manner and applying the remainder of the Hamiltonian operator (eq 11) reduces the problem to solution of the so-called *close-coupled* equations:

$$\frac{d^2}{d\rho^2}\mathbf{f}(\rho, \rho_i) + \mathbf{W}(\rho_i)\mathbf{f}(\rho, \rho_i) = 0 \qquad (15)$$

where the diagonal matrix **W** is given by (in atomic units)

$$W_{kk}(\rho_i) = 2\mu\left(E - \varepsilon_k(\rho_i) - \frac{3}{8\mu\rho_i^2} - \frac{J(J+1)}{2\mu\rho_i^2}\right) \qquad (16)$$

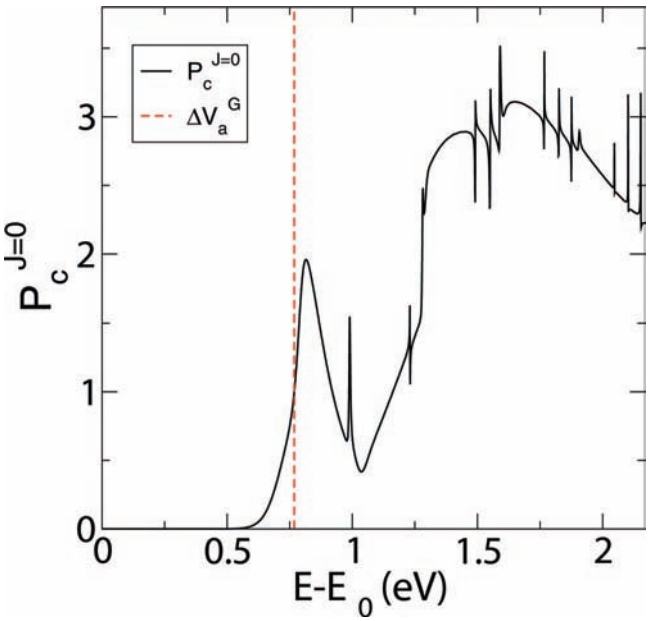

Figure 5. Cumulative reaction probability ($J = 0$) for the $CH_3 + CH_4$ reaction (solid line). The ab initio zero-point-corrected barrier height of $\Delta V_a^G = 0.768$ eV (dashed line) is included to highlight tunneling probability.

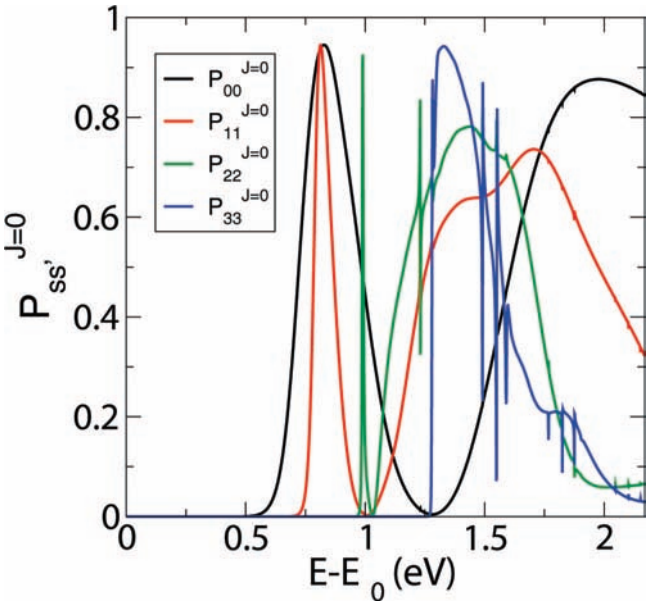

Figure 6. State-to-state reaction probabilities ($J = 0$) for $s \rightarrow s' = s$ for the $CH_3 + CH_4$ reaction.

Equation 15 is solved via an *R*-matrix propagation scheme,[33] whereby the *R*-matrix, formally defined as the ratio of the wave function and its outward normal gradient evaluated at the sector boundary,[33,42] is initiated in the interaction region and propagated through all sectors to asymptotic ρ. The method requires knowledge of the overlap matrix between adjacent sectors ρ_{i-1} and ρ_i, with matrix elements:

$$\mathcal{O}_{k'k} = \langle \phi_{k'}(\delta;\rho_{i-1}) | \phi_k(\delta;\rho_i) \rangle \tag{17}$$

The initial *R*-matrix propagation is performed for $J = 0$, and the overlap matrices and hyperspherical adiabats are stored for use in higher angular momenta calculations, which contributes greatly to the general efficiency of the method.

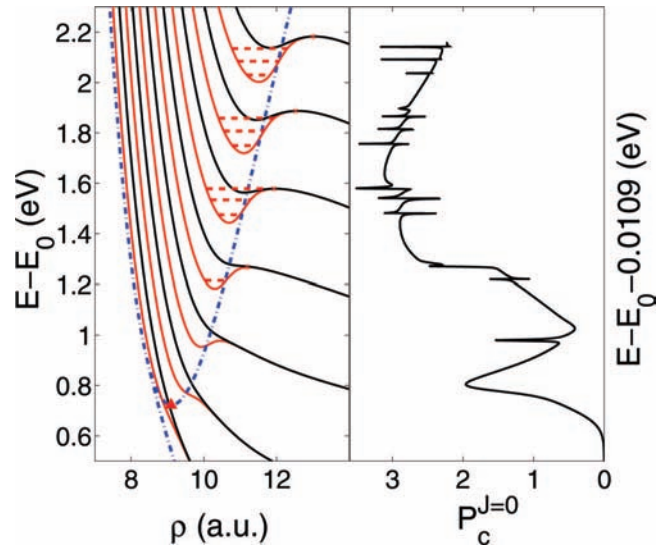

Figure 7. Right: Cumulative $J = 0$ reaction probability for the $CH_3 + CH_4$ reaction (solid line). Left: Hyperspherical adiabatic potentials in the interaction region (solid lines); potential minimum along product well and potential ridge (potential along ρ at fixed $\delta = (1/2)\delta_{max}$) (dotted blue lines); potential saddle point (surface TS) (Δ); and predicted metastable bound state energies (dashed red lines). The energy correction factor 0.0109 eV is applied to the cumulative reaction probability to allow correspondence between resonances and metastable bound state energies; this correction factor is intermediate between the initial ZPE in the asymptotic region and the ZPE of the infinitely separated reactants, and is most likely an effect of approximating the asymptotic region of ρ as consisting of noninteracting reactant molecules.

In the asymptotic region, approximate boundary conditions are applied directly in hyperspherical coordinates.[21,43] The *S*-matrix is extracted from the *R*-matrix by assuming incident (*I*) and outgoing (*O*) wave functions can be expressed as coming directly out of phase plane waves in ρ. For sector ρ_i (where a prime indicates the derivative of matrix elements with respect to ρ):

$$\mathbf{S}(\rho_i) = (\mathbf{R}(\rho_i)\mathbf{O}'(\rho_i) - \mathbf{O}(\rho_i))^{-1}(\mathbf{R}(\rho_i)\mathbf{I}'(\rho_i) - \mathbf{I}(\rho_i)) \tag{18}$$

$$I_{kk} = \lambda_k^{-1/2} \exp(-i\lambda_k\rho_i) \tag{19}$$

The elements of the diagonal matrix λ are defined as

$$O_{kk} = \lambda_k^{-1/2} \exp(i\lambda_k\rho_i) \tag{20}$$

$\lambda_k(\rho_i) = \sqrt{W_{kk}(\rho_i)}$ (defined for energetically accessible open channels only). The probability matrix elements, $P^J_{k'k}(E;\rho_i)$, for a given energy E and angular momentum J, are defined as the square modulus of the corresponding *S*-matrix elements. As only reactive transitions are of interest in this study, only probability matrix elements corresponding to transitions from initial reactant states (s) to final product states (s') are considered. The matrix P is therefore contracted to remove reactant to reactant and product to product transitions, and state-to-state reactive probability matrix elements are hereafter expressed as $P^J_{ss'}(E;\rho_i)$.

Ideally, $P^J_{ss'}(E;\rho_i)$ should be evaluated in the final sector only, thereby removing ρ_i dependence. However, applying approximate boundary conditions directly in hyperspherical coordinates can lead to oscillations in the state-to-state reaction probabilities as a function of sector ρ_i.[44] Therefore the *S*-matrix is calculated over an S_{num} number of sectors in the asymptotic

TABLE 7: Hyperspherical Adiabat Bound State Energies

transition	level	E (eV)
$\nu = 3$	0	1.2150
$\nu = 4$	0	1.4749
	1	1.5341
	2	1.5780
$\nu = 5$	0	1.7495
	1	1.8072
	2	1.8582
$\nu = 6$	0	2.0299
	1	2.0842
	2	2.1346

region, and the $P^J_{ss'}(E)$ is taken to be the average over the probability matrix elements in each of the final sectors.

Rate Constant and Cross Section Expressions. All dynamical and kinetic information presented in this study is derived from knowledge of the S and P matrices. For zero total angular momentum, summation over product states s′ and subsequently over reactant states s yields the $J = 0$ initial-state-selected ($P^{J=0}_s(E) = \sum_{s'} P^{J=0}_{ss'}(E)$) and cumulative reaction probabilities ($P^{J=0}_c(E) = \sum_s P^{J=0}_s(E)$), respectively. Dynamical and angular scattering information can be gleaned by calculation of the initial-state selected integral ($\sigma_s(E)$) and state-to-state differential ($\sigma_{ss'}(\theta)$) cross sections:

$$\sigma_s(E) = \frac{\pi}{{q_s}^2} \sum_{s'} \sum_{J=0}^{J_{max}} (2J + 1) P^J_{ss'}(E) \tag{21}$$

$$\sigma_{ss'}(\theta) = \frac{1}{4{q_s}^2} \left| \sum_J (2J + 1) S^J_{ss'} P_J(\cos\theta) \right|^2 \tag{22}$$

$${q_s}^2 = 2\mu_R(E - \varepsilon_s) \tag{23}$$

$$\mu_R = \frac{m_{CH_3} m_{CH_3H_a}}{m_{tot}} \tag{24}$$

These calculations require convergence with respect to J.

The total and state-to-state thermal rate constants are calculated by treating the spectator vibrational modes and the total angular momentum via energy and J-shifting approximations.[22,45,46] In the energy and J-shifting formalism, the cumulative reaction probability is given as: $P^J_c(E) \simeq P^{J=0}_c(E - E^{\#}_{rot} - E^{\#}_{vib})$, where $E^{\#}_{rot}$ and $E^{\#}_{vib}$ are the TS values for the rotational and spectator mode vibrational energy, respectively. This These assumption modifies the weighting factor outside the integral over the cumulative reaction probability function to include a ratio of TS and reactant electronic (Q_{elec}), vibrational (Q_{vib}), and rotational (Q_{rot}) partition functions:

$$k_{ss'}(T) = \frac{Q^{TS}_{int}}{2\pi Q^{CH_3}_{int} Q^{CH_3H_a}_{int} Q^{rel}_{trans}} \int_0^\infty dE P^{J=0}_{ss'}(E) e^{-E/k_B T} \tag{25}$$

$$k(T) = \frac{Q^{TS}_{int}}{2\pi Q^{CH_3}_{int} Q^{CH_3H_a}_{int} Q^{rel}_{trans}} \int_0^\infty dE P^{J=0}_{c}(E) e^{-E/k_B T} \tag{26}$$

$$Q_{int} = Q_{elec} \times Q_{vib} \times Q_{rot} \tag{27}$$

within the rigid rotor-harmonic oscillator approximation (in SI units):[18]

$$Q_{vib}(T) = \prod_{i=1}^{M} (1 - e^{-(\hbar\nu_i/k_B T)})^{-1} \tag{28}$$

$$Q_{rot}(T) = \frac{\sqrt{\pi}}{\sigma} \sqrt{\frac{T^3}{\Theta_a \Theta_b \Theta_c}} \tag{29}$$

$$\Theta_i = \frac{\hbar^2}{2 I_i k_B} \tag{30}$$

where M is the number of vibrations, ν the vibrational frequency, k_B is Boltzmann's constant, σ is the rotational symmetry number, Θ is the characteristic rotational temperature, and I is the moment of inertia.

Q^{rel}_{trans} is the relative translational energy partition function:

$$Q^{rel}_{trans}(T) = \left(\frac{m k_B T}{2\pi\hbar^2} \right)^{3/2} \tag{31}$$

$$m = \frac{m_{CH_3}(m_{CH_3H_a})}{m_{tot}} \tag{32}$$

The electronic partition functions are taken to be 2 and 1 for open and closed shell species to account for spin degeneracy, assuming that the separation between ground and excited electronic states is large enough to neglect electronically excited-state contributions.

The TST value of the thermal rate constant is also calculated in order to analyze the contribution of tunneling to the rate

TABLE 8: Thermal and State-to-State Rate Constants (cm^3 $molecule^{-1}$ s^{-1}, Powers of 10 in Parentheses)

T (K)	k_{tot}	k_{00}	k_{01}	k_{10}	k_{11}	k_{22}	k_{exp} [a]
250	1.23(−24)	1.22(−24)	6.20(−27)	6.19(−27)	8.65(−28)	1.01(−31)	
298	4.89(−23)	4.81(−23)	2.97(−25)	2.97(−25)	2.27(−25)	4.42(−29)	
350	1.16(−21)	1.12(−21)	7.97(−24)	7.96(−24)	1.81(−23)	7.06(−27)	1.17(−21)
400	1.33(−20)	1.26(−20)	1.01(−22)	1.01(−22)	4.31(−22)	3.31(−25)	1.45(−20)
500	5.21(−19)	4.72(−19)	4.68(−21)	4.68(−21)	3.86(−20)	9.16(−23)	4.94(−19)
600	7.22(−18)	6.23(−18)	7.53(−20)	7.53(−20)	8.20(−19)	1.77(−21)	5.19(−18)
800	2.47(−16)	1.97(−16)	3.26(−18)	3.26(−18)	4.18(−17)	4.53(−19)	9.80(−17)
1000	2.43(−15)	1.83(−15)	3.78(−17)	3.78(−17)	4.88(−16)	1.94(−17)	
1500	7.01(−14)	4.74(−14)	1.37(−15)	1.37(−15)	1.63(−14)	2.14(−15)	
2000	4.77(−13)	2.89(−13)	1.04(−14)	1.04(−14)	1.15(−13)	2.86(−14)	

[a] From ref 8.

constant:

$$k_{\mathrm{TST}}(T) = \frac{Q_{\mathrm{int}}^{\mathrm{TS}}}{2\pi Q_{\mathrm{int}}^{\mathrm{CH_3}} Q_{\mathrm{int}}^{\mathrm{CH_3H_a}} Q_{\mathrm{trans}}^{\mathrm{rel}}} \times k_{\mathrm{B}}T \times e^{-\Delta V_a^G/k_{\mathrm{B}}T} \quad (33)$$

The vibrational modes in eqs 25 and 26 are the $3N - 8$ projected modes, while the modes used in eq 33 are the $3N - 7$ unprojected modes (excluding the negative TS frequency). Multiple hydrogen abstraction sites are accounted for in both the scattering and TST thermal rate constants by the symmetry number σ in the rotational partition function.

Numerical Details. A series of calculations were performed to test the convergence of cumulative probabilities and reaction cross sections with respect to scattering parameters N_δ, N_ρ, $J_{\max}$, and E_{inc}. The hyperspherical adiabats were found to have minimal oscillatory behavior in the asymptotic region, and therefore S_{num} was fixed to the final 15% of N_ρ based upon the experience of previous studies.[18,21] The parameters used in our quantum scattering calculations are given in Table 6.

Results

Reaction Probabilities and Resonances. Cumulative and state-to-state reaction probabilities for $s \rightarrow s' = s$ are shown in Figure 5 and Figure 6, respectively. The ab initio barrier (17.7 kcal/mol, 0.768 eV) is included in Figure 5 to highlight the significance of tunneling for the $0 \rightarrow 0$ transition. The overlap of the $0 \rightarrow 0$ and $1 \rightarrow 1$ transitions is explained by analyzing the hyperspherical adiabats (Figure 7), where it is shown that the saddle point (surface TS) along the potential ridge of $\delta_{\max}/2$ is reached just before the higher energy channel becomes accessible, causing an almost simultaneous opening of the two channels. Transitions with $s' \neq s$ contribute minimally to the cumulative reaction probability and are therefore not shown.

The state-to-state reaction probabilities (Figure 6) exhibit oscillating reactivity, a phenomenon studied extensively for triatomic HLH reactions in classical, semiclassical, and quantum approximations,[31,47] although the feature here is most visible for the ground-state transition. Oscillating reactivity has been shown to occur as a result of quantum interference between wave functions on the asymptotically degenerate *gerade* and *ungerade* adiabatic potentials.[31] This same pattern is shown in Figure 7, although in the current study the hyperspherical adiabats shown are not true *ungerade* and *gerade* states, as the symmetry was not explicitly treated in the scattering calculations. The strong resonances[31] observed in the cumulative reaction probability were characterized by solving the Schrödinger equation for the hyperspherical adiabat potentials in a DVR basis,[40] by restricting the ρ interval of each metastable potential to less than the value at the local maximum. Computed energies in comparison to shifted $P_c^{J=0}$ show correspondence between resonances and interaction region bound states, thus allowing for a semiquantitative description of the metastable bound states. The energies of the calculated bound states are given in Table 7. Much research has been done on the bound states of symmetric triatomic reactions such I + HI, where so-called vibrationally bonded states have been indicated.[48] Although the title reaction shows bound state resonances only for transitions from $v = 3$ or higher, characterization of these bound states is useful in providing a means for physical interpretation of $P_c^{J=0}$ with respect to the vibrations of the system's active modes. Population of a vibrationally excited metastable bound state occurs when the incident kinetic energy coincides with the frequency of vibrational motion in the hyperspherical coordinate ρ, corresponding to the trapping of energy in vibrations involving motion between the two heavy groups, $CH_3(1)$ and $CH_3(2)$.

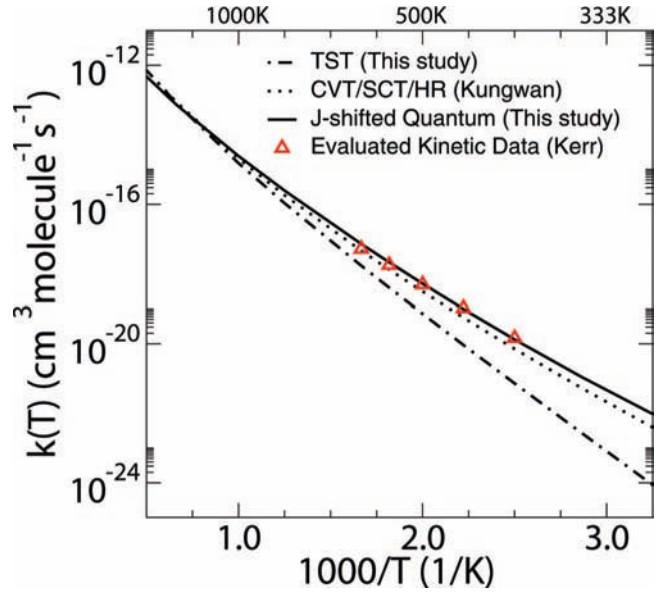

Figure 8. Thermal rate constants for the $CH_3 + CH_4$ reaction. Evaluated experimental kinetic data (Δ) and CVT/SCT/HR theoretical results (dotted line) are taken from Kerr (1976) and Kungwan (2005), respectively.

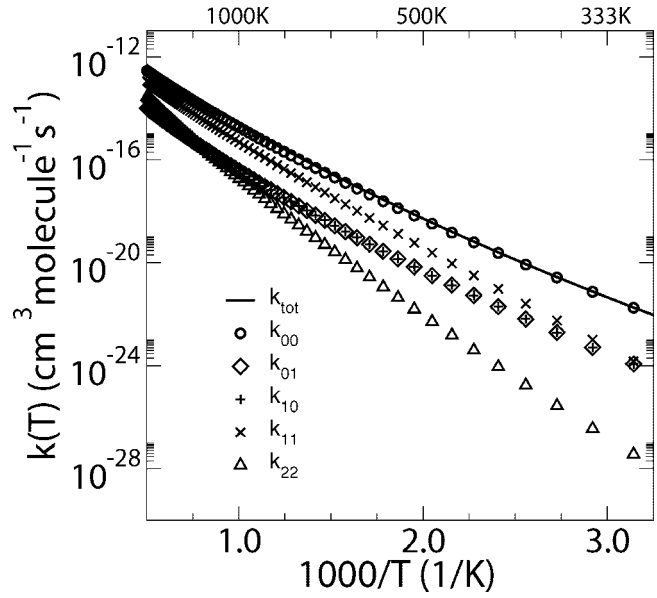

Figure 9. State-to-state thermal rate constants for the $CH_3 + CH_4$ reaction.

Thermal and State-to-State Rate Constants. The total and state-to-state thermal rate constants are presented in Figure 8, Figure 9, and Table 8. The total thermal rate constant is shown in comparison to TST (this study), CVT/SCT with hindered rotor (HR) treatment,[2] and evaluated kinetic data.[8] Deviation of the scattering results from TST indicate that tunneling plays an important role in the low temperature region, a conclusion supported by the fact that the rate constant of the $0 \rightarrow 0$ transition ($k_{0\rightarrow 0}$), which dominates the total thermal rate constant $k(T)$ (Figure 8), opens at energies below the ab initio barrier height. Contributions of nonadiabatic transitions between the ground and the first excited vibrational states to the total rate

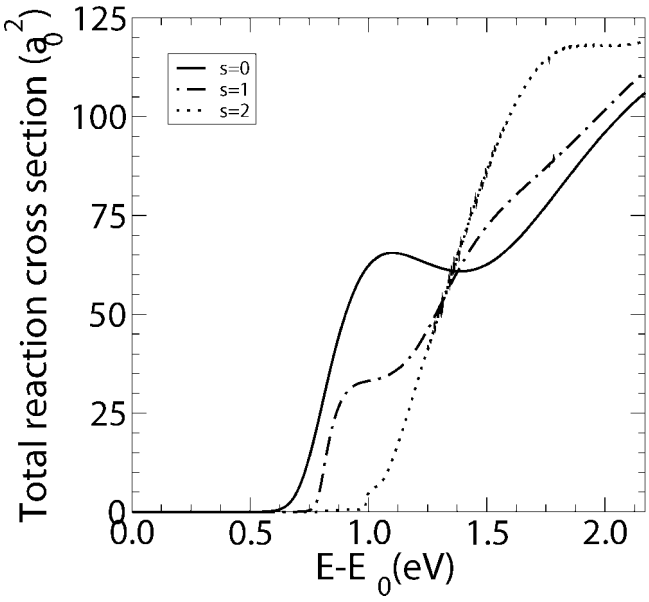

Figure 10. Initial state-selected integral reaction cross section for the $CH_3 + CH_4$ reaction.

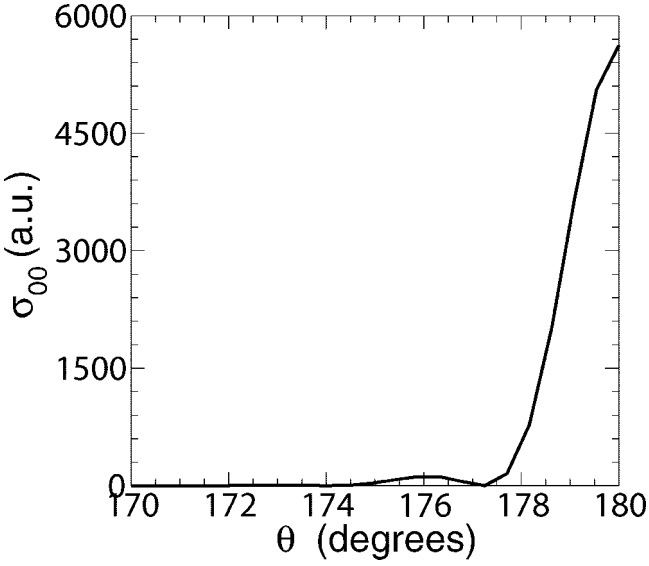

Figure 11. $0 \rightarrow 0$ differential cross section for the $CH_3 + CH_4$ reaction: shown for 0.886 eV, the energy resulting in the maximum differential cross section amplitude.

constant are greater than an order of magnitude smaller than the $0 \rightarrow 0$ transition across the entire temperature range.

Figure 8 shows a close correspondence between the evaluated kinetic data of Kerr[8] and the CVT/SCT/HR data of Kungwan,[2] but the CVT results are slightly below the experimental and current values at low temperatures. The 2D quantum scattering results of the current study agree quite well with the evaluated kinetic data and represent a significant improvement upon the classical TST approaches. This improvement is most visible at low temperatures, although the quantum scattering results also predict a small degree of high-temperature recrossing not included in the classical TST models.

Cross Sections. The initial state-selected integral cross sections (Figure 10) show the opening of the ground and first excited states in quick succession. The comparatively delayed opening of the second excited-state channel is consistent with the energy of its associated hyperspherical adiabat and consistent with the first large increase in $P_{22}^{J=0}$ (Figure 7 and Figure 6, respectively).

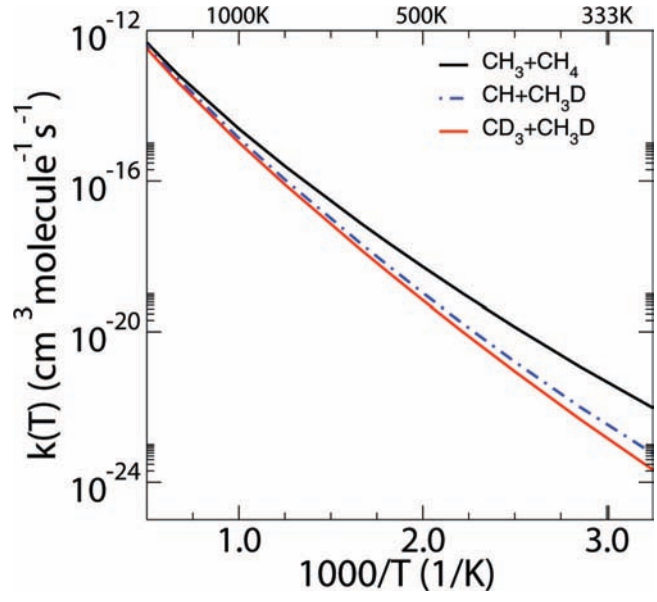

Figure 12. Thermal rate constant comparison for the $CH_3 + CH_4$ reaction and deuterium-substituted reactions $CD_3 + CD_4$ and $CH_3 + CH_3D$.

TABLE 9: Kinetic Isotope Effect: Ratio of Substituted System to Title Reaction

T (K)	$CH_3 + CH_3D$ ($4k_2/k_1$)	$CD_3 + CD_4$ (k_3/k_1)
300	0.0564	0.0199
350	0.0847	0.0400
400	0.1203	0.0663
450	0.1604	0.0968
500	0.2023	0.1296
550	0.2445	0.1636
600	0.2860	0.1976
800	0.4383	0.3255
1000	0.5639	0.4327
1500	0.7718	0.6103
2000	0.8697	0.6975
2500	0.9060	0.7386

The $0 \rightarrow 0$ differential cross section was also evaluated according to eq 22. The reaction was found to be exclusively backward scattering for all incident kinetic energies. A sample differential cross section is given for $E - E_0 = 0.886$ eV in Figure 11, for which maximum differential cross section amplitude was observed.

Kinetic Isotope Effects. Primary and secondary KIEs were investigated for reactions 2 and 3 (Figure 12, Table 9). The difference in reactant rotational symmetry numbers in the rotational partition function prefactor causes a factor of 4 decrease in the rates of the $CH_3 + CH_3D$ (k_2) reaction in comparison to the $CD_3 + CD_3$ (k_3) and the title reaction. Thus, correction of k_2 by a factor of 4 affords comparison of reaction rate excluding rotational symmetry effects. It is shown that both substitutions decrease the reaction rate considerably in the low temperature regime, indicating an expected decrease in tunneling for transfer of deuterium (Figure 12). However, despite the higher ab initio barrier height of reaction 2 compared to 3, k_3 is lower than the factor of 4 scaled k_2 because of the ZPE differences on the PES that result in a narrower reaction barrier and thus increased tunneling. Therefore secondary isotope effects are seen to contribute—albeit minimally in comparison to the primary effect—to a decrease in the reaction rate at low temperatures.

Conclusions

2D quantum scattering calculations were performed on fitted ab initio PESs for the symmetric hydrogen exchange $CH_3 + CH_4 \rightarrow CH_4 + CH_3$ and two symmetric deuterium substitutions. The reaction probabilities and hyperspherical adiabats of the symmetric title reaction were explored with respect to oscillating reactivity, and bound states were quantitatively analyzed with respect to resonances. We find that the 2D method used in this study compares well with the experimental rate constants. The KIEs are reported, and only small contributions are found from secondary KIEs, with the majority of the effects attributed to substitution of the transferring atom. Finally, it must be noted that this reaction forms a basis from which to understand fundamental bimolecular hydrogen transfer reactions, especially for hydrocarbon systems.[2] This study provides additional dynamical information that might also be relevant in interpreting the dynamics within its reaction class. The ability to apply an RD method to a system such as this indicates that treatment of the two active modes is a good approximation, and this study is an important step in validating the use of the method for large HLH hydrogen exchange processes. Application of this method to bimolecular hydrogen exchange processes will be extended to larger systems in future studies.

Acknowledgment. This work was supported by the United States Office for Naval Research (Grant N00014-05-1-0460) and the Engineering and Physical Sciences Research Council (Grant Number EP/G00224X/1). S.M.R. acknowledges the Oxford University Press through receipt of a Clarendon Scholarship for support of graduate study. S.T.B. thanks the Ramsay Memorial Fellowship Trust for support through a Ramsay Memorial Fellowship.

References and Notes

(1) Back, M. H.; Back, R. A. *Pyrolisis: Theory and Industrial Practice*; Academic Press, Inc.: New York, 1983.
(2) Kungwan, N.; Truong, T. N. *J. Phys. Chem. A* **2005**, *109*, 7742–7750.
(3) McNesby, J.; Gordon, A. *J. Am. Chem. Soc.* **1954**, *76*, 4196–4198.
(4) Derwish, G.; Galli, A.; Giardini-Guidoni, A.; Volpi, G. *J. Chem. Phys.* **1964**, *40*, 5–12.
(5) Dainton, F.; McElcheran, D. *J. Chem. Soc., Faraday Trans.* **1955**, *51*, 657–664.
(6) Dainton, F.; Ivin, K.; Wilkinson, F. *J. Chem. Soc., Faraday Trans.* **1959**, *55*, 929–936.
(7) Dainton, F.; Ivin, K.; Wilkinson, F. *Spec. Pub. Chem. Soc.* **1958**, *9*, 187–195.
(8) Kerr, J.; Parsonage, M. *Evaluated Kinetic Data on Gas Phase Hydrogen Transfer Reactions of Methyl Radicals*; Butterworths: London, 1976.
(9) Arthur, N.; Bell, T. *Rev. Chem. Intermed.* **1978**, *2*, 37–74.
(10) Canadell, E.; Olivella, S.; Poblet, J. M. *J. Phys. Chem.* **1984**, *88*, 3545–3549.
(11) Chandra, A. K.; Malar, E. P.; Gupta, D. S. *Int. J. Quantum Chem.* **1992**, *41*, 371–379.
(12) Fradera, X.; Duran, M.; Mestres, J. *Can. J. Chem.* **2000**, *78*, 328–337.
(13) Gillion, R. D. *J. Comput. Chem.* **1984**, *5*, 237–240.
(14) Jursic, B. S. *Chem. Phys. Lett.* **1995**, *244*, 263–268.
(15) Litwinowicz, J.; Ewing, D.; Jurisevic, S. *J. Phys. Chem.* **1995**, *99*, 9709–9716.
(16) Mestres, J.; Duran, M.; Bertran, J. *Can. J. Chem.* **1996**, *74*, 1253–1262.
(17) Pederson, M. R. *Chem. Phys. Lett.* **1994**, *230*, 54–60.
(18) Kerkeni, B.; Clary, D. C. *J. Chem. Phys.* **2004**, *120*, 2308–2318.
(19) Kerkeni, B.; Clary, D. C. *Mol. Phys.* **2005**, *103*, 1745–1755.
(20) Kerkeni, B.; Clary, D. C. *Chem. Phys. Lett.* **2007**, *438*, 1–7.
(21) Banks, S. T.; Clary, D. C. *Phys. Chem. Chem. Phys.* **2007**, *9*, 933–943.
(22) Bowman, J. M. *Theor. Chem. Acc.* **2002**, *108*, 125–133.
(23) Althorpe, S. C.; Clary, D. C. *Annu. Rev. Phys. Chem.* **2003**, *54*, 493–529.
(24) Wang, Y.; Braams, B.; Bowman, J. M.; Carter, S.; Tew, D. P. *J. Chem. Phys.* **2008**, *128*, 224314.
(25) Truhlar, D. G.; Garrett, B. C.; Klippenstein, S. J. *J. Phys. Chem.* **1996**, *100*, 12771–12800.
(26) Bowman, J. M. *Adv. Chem. Phys.* **1985**, *61*, 115.
(27) Bowman, J. M.; Wagner, A. Reduced Dimensionality Theories of Quantum Reactive Scattering: Applications to Mu + H2, H + H2, O(3P)+H2, D2 and HD. In *The Theory of Chemical Reaction Dynamics*; Clary, D. C., Ed.; D. Riedel Publishing Company: Dordrecht, 1986; p 47.
(28) Tautermann, C. S.; Wellenzohn, B.; Clary, D. C. *Mol. Phys.* **2006**, *104*, 151–158.
(29) Walker, R. B.; Hayes, E. F. Reactive Scattering in the Bending Corrected Rotating Linear Model. In *The Theory of Chemical Reaction Dynamics*; Clary, D. C., Ed.; D. Reidel Publishing Company: Dordrecht, 1986; p 105.
(30) Banks, S. T.; Clary, D. C. *J. Chem. Phys.* **2009**, *130*, 024106.
(31) Romelt, J. Calculations on Collinear Reactions using Hyperspherical Coordinates. In *The Theory of Chemical Reaction Dynamics*; Clary, D. C., Ed.; D. Riedel Publishing Company: Dordrecht, 1986; p 77
(32) Clary, D. C. *Phys. Chem. Chem. Phys.* **1999**, *1*, 1173–1179.
(33) Stechel, E.; Walker, R. B.; Light, J. C. *J. Chem. Phys.* **1978**, *69*, 3518.
(34) Frisch, M. J.; Trucks, G. W.; Schlegel, H. B.; Scuseria, G. E.; Robb, M. A.; Cheeseman, J. R.; Montgomery, J. A., Jr.; Vreven, T.; Kudin, K. N.; Burant, J. C.; Millam, J. M.; Iyengar, S. S.; Tomasi, J.; Barone, V.; Mennucci, B.; Cossi, M.; Scalmani, G.; Rega, N.; Petersson, G. A.; Nakatsuji, H.; Hada, M.; Ehara, M.; Toyota, K.; Fukuda, R.; Hasegawa, J.; Ishida, M.; Nakajima, T.; Honda, Y.; Kitao, O.; Nakai, H.; Klene, M.; Li, X.; Knox, J. E.; Hratchian, H. P.; Cross, J. B.; Bakken, V.; Adamo, C.; Jaramillo, J.; Gomperts, R.; Stratmann, R. E.; Yazyev, O.; Austin, A. J.; Cammi, R.; Pomelli, C.; Ochterski, J. W.; Ayala, P. Y.; Morokuma, K.; Voth, G. A.; Salvador, P.; Dannenberg, J. J.; Zakrzewski, V. G.; Dapprich, S.; Daniels, A. D.; Strain, M. C.; Farkas, O.; Malick, D. K.; Rabuck, A. D.; Raghavachari, K.; Foresman, J. B.; Ortiz, J. V.; Cui, Q.; Baboul, A. G.; Clifford, S.; Cioslowski, J.; Stefanov, B. B.; Liu, G.; Liashenko, A.; Piskorz, P.; Komaromi, I.; Martin, R. L.; Fox, D. J.; Keith, T.; Al-Laham, M. A.; Peng, C. Y.; Nanayakkara, A.; Challacombe, M.; Gill, P. M. W.; Johnson, B.; Chen, W.; Wong, M. W.; Gonzalez, C.; Pople, J. A. *Gaussian 03*, revision C.02; Gaussian, Inc.: Wallingford, CT, 2004.
(35) Jayatilaka, D.; Lee, T. J. *J. Chem. Phys.* **1993**, *98*, 9734–9747.
(36) Lee, T. J.; Rice, J. E.; Scuseria, G. E.; Schaefer, H. F. I. *Theor. Chim. Acta* **1989**, *75*, 81–98.
(37) Jensen, F. *Introduction to Computational Chemistry*; John Wiley and Sons: Chichester, 2004.
(38) Lu, D.-h.; Truhlar, D. G. *J. Chem. Phys.* **1993**, *99*, 2723–2730.
(39) *Matlab*, version 7.1.0.183 (R14) Service Pack 3; The MathWorks, Inc.: Natick, MA, 2007 (copyright 1984−2005).
(40) Muckerman, J. T. *Chem. Phys. Lett.* **1990**, *173*, 200.
(41) Hernandez, M. I.; Campos-Martinez, J.; Villarreal, P.; Schmatz, S.; Clary, D. C. *Phys. Chem. Chem. Phys.* **1999**, *1*, 1197–1203.
(42) Light, J. C. The R-matrix Method. In *The Theory of Chemical Reaction Dynamics*; Clary, D. C., Ed.; D. Reidel Publishing Company: Dordrecht, 1986; pp 215−234.
(43) Brooks, A.; Clary, D. C. *J. Chem. Phys.* **1990**, *92*, 4178–4190.
(44) Nyman, G.; Yu, H. G. *Rep. Prog. Phys.* **2000**, *63*, 1001–1059.
(45) Bowman, J. M. Approximate Time Independent Methods for Polyatomic Reactions. In *Reaction and Molecular Dynamics: Proceedings of the European School on Computational Chemistry*; Lagana, A., Riganelli, A., Eds.; Springer-Verlag: New York, 2000; p 101.
(46) Bowman, J. M. *J. Phys. Chem.* **1991**, *95*, 4960–4968.
(47) Aquilanti, V. Resonances in Reactions: A Semiclassical View. In *The Theory of Chemical Reaction Dynamics*; Clary, D. C., Ed.; D. Reidel Publishing Company: Dordrecht, 1986; pp 383−413.
(48) Clary, D. C.; Connor, J. *Chem. Phys. Lett.* **1983**, *94*, 81.

JP810803K